Title
IN-BEAM NUCLEAR GAMMA-RAY STUDIES OF RELATIVISTIC HEAVY ION REACTIONS

Permalink
https://escholarship.org/uc/item/0qq2z1rb

Author
Shibata, T.

Publication Date
1978-02-01

Submitted to Nuclear Physics A

LBL-7189 c.2
Preprint

IN-BEAM NUCLEAR GAMMA-RAY STUDIES OF RELATIVISTIC HEAVY ION REACTIONS

T. Shibata, H. Ejiri, J. Chiba, S. Nagamiya,
K. Nakai, R. Anholt, H. Bowman, J. G. Ioannou,
E. A. Rauscher and J. O. Rasmussen

February 1978

Prepared for the U. S. Department of Energy
under Contract W-7405-ENG-48

LBL-7189

In-beam Nuclear Gamma-Ray Studies of Relativistic Heavy Ion Reactions[+]

T. Shibata and H. Ejiri

Department of Physics, Osaka University and
Lawrence Berkeley Laboratory, University of California

J. Chiba, S. Nagamiya and K. Nakai

Department of Physics, University of Tokyo and
Lawrence Berkeley Laboratory, University of California

and

R. Anholt[*] H. Bowman, J.G. Ioannou, E.A. Rauscher and J.O. Rasmussen

Lawrence Berkeley Laboratory, University of California
Berkeley, California 94720

Abstract:

Discrete nuclear γ-rays following interactions of relativistic ^{12}C and alpha projectiles with Sr, Na, S and Ca targets were measured in-beam with Ge(Li) detectors. The observed γ-rays were mostly due to the first excited-state-to-ground transitions of target fragments produced in peripheral collisions of the heavy ions. Characteristic features of the peripheral process consistent with the projectile-fragment studies were observed. The general behavior of the reactions was qualitatively understood with a picture of a fast-cascade followed by evaporation.

†This work was supported by the Physical Research Division of the U.S. Department of Energy, the Mitsubishi Foundation (Japan), the Japanese Society for the Promotion of Science, and had the endorsement of the National Science Foundation.

*Present address: Gesellschaft für Schwerionenphysik, Darmstadt, West Germany.

Key Words: E NUCLEAR REACTIONS

Sr, (^{12}C, Xγ), $E_{^{12}C}$ = 3, 12.6 GeV

Na, S, Ca(^{12}C, Xγ) E = 3, 4.8 GeV,

Na, S, Ca(α, Xγ) E_α = 1.6 GeV; measured $\sigma(E\gamma)$ Iγ; Natural targets.

1. Introduction

In-beam nuclear gamma spectroscopy has extensively been carried out to study medium-heavy nuclear structure. Reactions proceed by compound-nucleus formation with low energy projectiles($\leq$10 MeV/nucleon). Nuclear reactions with medium and high energy projectiles are rather non-compound, so that de-excitation via the pre-equilibrium process becomes important. The purpose of the present work is to extend in-beam gamma spectroscopy to high energy (relativistic) heavy ion projectiles. The observation of the discrete γ-rays is useful to study the mechanism of the target fragmentation in the peripheral collision process with rather small energy and momentum transfer.

The peripheral process in the relativistic heavy ion collision has been studied by observing projectile fragmentation[1,2]. Evidence for fragmentation includes the observvtions of the transferred momentum distributions and the cross sections for the projectile fragments.

Similarities in the asymptotic behavior of the fragmentation processes between relativistic heavy ion reactions and ultra high energy hadronic reactions have been shown[2,3]. Another similarity was shown for fragmentation cross sections between 2.1-GeV/N and 20-MeV/N ^{16}O projectiles[4]. Several theoretical works on the reaction mechanism have appeared[5-9]. The knowledge of such high - energy heavy ion reactions has, until the very recent work of Lindström, _et_ _al_., on ^{56}Fe beams[10], been limited to results with low mass projectiles (A≤16). Studies of target fragmentation give complementary information on the reaction mechanism. The observation of prompt and delayed nuclear γ-rays from target residues following reactions with relativistic projectiles is most applicable for the study of the target fragmentation in the target mass range from ~20-40. There are not very many suitable radioactive species for off-line counting in this region, so off-line techniques are more applicable for heavier targets (see ref. 11). Furthermore, projectile fragmentation techniques in the mass range above 20 have difficulty in resolving isotopes.

In-beam γ-rays following light-ion projectiles with medium and high energies have been studied by several groups. The reactions with medium-energy protons and alphas have been found to proceed firstly through particle de-excitation at the pre-equilibrium stage, being followed later by the evaporation process at the equilibrium stage.12) Nuclear γ-rays following relativistic proton and pion bombardments have been reported.13-19) However, there has been no work on in-beam γ-rays with relativistic heavy ions.

In this work we measured for the first time discrete γ-rays from excited residual nuclei produced in relativistic heavy ion reactions. The observation of γ-rays may give the following information:

1) production cross sections of target fragments from observation of characteristic γ-transitions in product nuclei,

2) momentum transfer in target fragments from the Doppler broadening (or shift) of lines in γ-ray spectra,

3) angular momentum transfer from yield ratios between high-spin and low-spin states in the products, and

4) nuclear orientation effects in the reaction from observation of γ-ray angular distributions.

These are important for understanding the reaction mechanisms involved.

In this paper we report on the production cross sections and briefly on the transverse-momentum transfer implied by Doppler broadening of gamma lines.

2. Experimental Procedure

Relativistic carbon and alpha beams from the Bevatron at Lawrence Berkeley Laboratory were used on various targets. Low energy nuclear γ-rays following nuclear reactions were observed with Ge(Li) detectors. A typical set-up of experiments is shown in Fig. 1.

The beam spot was about 2 cm in diameter. Typical time structures of the beam are shown in Fig. 2. The beam spill was about 1 second in every 4-6 seconds. Depending upon the mode of operation during the spill, we are able to choose a beam either with or without microscopic structure. When the r.f. power for the accelerator resonator is turned off during the spill, a continuous beam is available, a desirable feature for coincidence experiments. The extraction can be made also with the r.f. power on so that the microscopic beam structure can be used. In this case, pulsed beams, having an interval of 450-550 ns, depending on the beam energy, are available. We were able to take three different spectra, "prompt," "delayed" (between the micro bursts) and "off-beam" (between spills), as shown in Fig. 2.

The beam intensity was monitored with an ion chamber which was calibrated by measuring the ^{11}C radioactivity produced in graphite targets by the $^{12}C(X,X'n)^{11}C$ reaction. The ^{11}C-production cross section is available for the $^{12}C(^{12}C, ^{11}C)X$ reaction at $E(^{12}C) = 12.6$ Gev $^{2)}$. For the other energies, we estimated the ^{11}C production cross section from the results of the $^{12}C(p, X)^{11}C$ $^{20)}$, $^{12}C(Ne, X)^{11}C$ $^{21)}$ and $^{12}C(^{12}C, ^{11}C)X$ $^{2)}$ reactions. In an earlier run (Run 1) the absolute cross sections were determined relative to the x-ray yield, since the ion chamber was placed behind the thick target, and it was later found that the current was affected by the secondary particles produced in the target. A thin gold foil was located 10 cm upstream from the target location. Gamma-ray yields were then determined relative to the known x-ray cross section for the gold target $^{22)}$.

We had three major runs, Runs 1, 2 and 3, following a few initial trial runs. The experimental conditions are summarized in Table 1. The first run was a survey run in which we tried to observe in-beam γ-rays from various excited states of light, medium and heavy nuclei. In the second run, however, we decided to focus the measurements on light nuclei in order to study target-fragmentation mechanisms. In this run we learned that the effect of secondary particles was not trivial, as discussed in a later section and the appendix.

Based on experience from the earlier runs, we improved experimental conditions substantially in the third run. We used a PDP-11/10 computer with a CAMAC interface, which made it possible to take 6 x 2.048k spectra and 12-channel scaler counts. Using the micro- and macro-beam structure, we were able to take prompt, delayed and off-beam γ-ray spectra with two Ge(Li) detectors.

The beam intensity was adjusted to keep the average counting rates of the Ge(Li) detectors about 4 kcps. The maximum counting rate was dependent on the uniformity of the beam intensity during the one-second beam spill. The fluctuation of the beam intensity on a millisecond time scale during the beam spill was sufficiently large that the dead-time correction was substantial in spite of the average low counting rate. The dead-time correction was made by counting a pulser peak in the spectrum, with the pulser triggered by the scaled-down pulses from a NaI(Tl) detector placed at a different angle to the beam axis.

Another difficulty was due to large pulses which blanked out the Ge(Li) detectors. Those were due to high energy particles from the targets or the beam halo. Though the beam spot on the target was about 2 cm in diameter, we observed beam halo due to scattered beam or secondary particles. We attempted to reduce the beam halo effect by adjusting the target-to-detector distance, putting absorbers (Lucite) between them, putting beam-particle collimators upstream of the target, and so on. None of these methods cleaned up the pulses appreciably, and we had to run with the detectors at large distances from the target (~15 cm) and at relatively low counting rates.

Since the Bevatron cave had been used for so many years, the radioactive background was high. Several characteristic γ-lines from long-lived radioactivities such as ^{22}Na, and ^{60}Co were observed. In order to improve signal-to-background ratios under such circumstances, we needed to use fairly thick targets. Then, effects of reactions in the target by secondary particles from the heavy ion reaction became large, and we had to correct for such effects. For determination of the correction we used targets with different thicknesses. We will discuss this in more detail in the appendix.

3. Results

Many discrete γ-rays following relativistic ^{12}C- and α-induced nuclear reactions on various targets were successfully observed. Representative γ-ray spectra are shown in Figs. 3-5. Identification of the γ-rays was made by referring to known γ-ray energies. The strong "continuum background" was established as largely target-associated, since it dropped during target-out runs. It probably arises from Compton events from high energy gamma rays and from numerous weak unresolved lower energy transitions.

The uncertainty of the γ-ray cross section is due to the uncertainties in detector efficiency, target thickness, beam flux, the dead-time correction, and the correction for secondary effects. The estimated uncertainty of absolute cross sections for Run 3 was 15-17% in addition to the statistical error, and 35% for Run 1. Only relative yields were obtained for Run 2. The obtained cross sections (or relative intensities) are summarized in Tables 2 to 5. Some target-associated γ-rays were identified in the off-beam spectra, which were measured between the one-second beam spills. These γ-rays arise from radioactive products with half lives longer than 1 sec. From these γ-rays we were able to determine the cross sections of a few parent nuclei. The results are listed in Table 6.

We did not observe significant anisotropy of γ-rays within error limits.

The following observations should be mentioned:

1) The γ-ray peak-to-continuum background ratios were better in light-mass targets than in heavier-mass targets. This may be due to the fact that the number of various target fragments from heavy-mass targets is much larger than those from light-mass targets. Therefore, the γ-rays from a heavy-mass target arise from so many kinds of fragments that only very intense γ-rays from the fragments in the vicinity of the target nucleus show up above the continuum.

Furthermore, the ratio of central collisions to total collisions is larger in the heavy mass target, resulting in more unresolved γ-rays from the central collision.

2) Gamma-rays from short-lived states in light mass nuclei (A = 20-40) are Doppler broadened. Most of the γ-rays for the Sr target, however, are not Doppler broadened beyond the intrinsic resolution because of the heavier masses and longer lifetimes in comparison with the sd shell nuclei. It should be mentioned that all γ-rays observed from light mass targets come from the de-excitation of excited states with half lives longer than 250 fs. This may be due to the fact that high energy γ-rays (>1 MeV) from very short-lived states (<100 fs) have large Doppler broadening, resulting in broader peaks which cannot be seen in the spectrum.

4. Discussion

4.1 Q-value dependence of discrete γ-rays

The measured γ-ray intensity for a particular transition represents a fraction of the total yield of a nuclide, depending on the pattern of γ-transition feeding from higher excited states. In a doubly even nucleus, however, most excited states below the particle separation energy de-excite through the first 2^+ state by γ-decay. If we assume equal population for all excited states, we can estimate the fraction of the total yield for the $2^+ \rightarrow 0^+$ transition using γ-ray branching ratios[23]. The $2^+ \rightarrow 0^+$ gamma ray yield may collect 70 ~ 80% of the total yield for most of the measured doubly even nuclei. Since the evaporation process, as we discuss later, is important at the final stage of the reaction, many excited states are formed after particle evaporation, and one may neglect the direct formation of the ground state. Thus, we concentrate our attention here on the yields of the $2^+ \rightarrow 0^+$ transitions in doubly even products. In fig. 6, we show the relative yields for ^{12}C at 250 MeV/N on the Na, S, and Ca targets. We have taken as abscissa the negative value of the minimum Q value (the minimum excitation energy of the target nucleus)[8] to form the given product among the Q values for various ways, such as multiple nucleon and alpha removal, two-body break-up (fission), etc. In Fig. 6, we see a monotonic decrease of yield with increasing magnitude of Q_{min}. In Fig. 7, we see the corresponding plot for the higher bombarding energy data at 400 MeV/N. The slopes of the exponential decrease of the yields with $|Q_{min}|$ at 400 MeV/N are less than those at 250 MeV/N. In other words the product nuclei go further from the target mass at 400 MeV/N. Notable exceptions to the correlation with $|Q_{min}|$ are the yields of ^{18}O from the ^{23}Na target and ^{32}Si from the Ca target. In the former case the yield of ^{18}O is unusually low, though it can be reached by a simple knockout or evaporation (2 p and 1 α) from ^{23}Na. This may be partly due to the rather small difference between the neutron separation energy (10.4 MeV) and the proton separation energy (8 MeV) for ^{19}F. Thus because of the Coulomb barrier (~3 MeV) for proton emission, excited states above the neutron separation energy in ^{19}F preferentially decay to ^{18}F by neutron emission rather than to ^{18}O. In the case of the ^{32}Si residual nucleus from the Ca target the yield is rather high for the simple correlation with $|Q_{min}|$. This is the only observed product with $|T_z| = 2$. The recent calculation by Rasmussen, et al.,[24] fails to explain this large cross section. We cannot exclude possible contaminant γ-rays that would lower this unusually high yield.

Note that no products with mass number greater than the target are ever observed. At these high energies, evidently,neither compound nucleus formation nor nuclear or cluster transfer processes exhibit measurable cross sections.

In-beam gammameasurements[25)] with 90-MeV alpha particles on calcium do show heavier products, such as ^{42}Ca. It appears likely that nucleon transfer in the high energy region will fall off with increasing projectile velocity according to the momentum mismatch of the nucleon in the nucleus. That is, for beam energies above the Fermi energy of 50 MeV/N transfer will become small.

4.2 Comparison of γ-ray yields between α and ^{12}C bombardments

The alpha bombardment data at 400 MeV/N gave relative yields very similar to those of the carbon-ion run at the same velocity. Only the absolute cross sections change somewhat. In Fig. 8 we have plotted the ratio of cross sections with ^{12}C to those with alphas at 400 MeV/N. Only products where the error limits are not too large are shown and within error almost all points are consistent with a ratio of ~1.2. Lindström, *et al.*,[2)] have shown projectile fragmentation cross sections to have a mass dependence of $\sigma = C(A_p^{1/3} + A_t^{1/3} - 1.6)$, characteristic of a peripheral process, with C a constant. With their expression we calculate ^{12}C-to-α ratios of 1.25, 1.22, and 1.21, respectively, for the ^{23}Na, ^{32}S, and ^{40}Ca targets. The experimental ratio appears to deviate from the expression for the product ^{20}Ne at half the mass of its target ^{40}Ca.

4.3 Asymmetry in the proton and neutron removal probability

We noted that the γ-rays observed in the Na, S and Ca targets, with $T_z = 0$ or $1/2$, were mostly from product nuclei with $T_z = 0$, $1/2$ or 1. Gamma-rays from products with $T_z = -1/2$ were rare. In other words, protons are more likely to be removed than neutrons from these light nuclei. On the other hand, γ-rays from the Sr target were mostly from products of neutron removal reactions. We observed no γ-rays in ^{84}Kr which can be produced by a single α knock-out reaction. The upper limit for the yield of the $2^+ \rightarrow 0^+$ transition in ^{84}Kr was one third that of the $2^+ \rightarrow 0^+$ transition in ^{84}Sr. These facts suggest the importance of the evaporation process. That is, the proton separation energy is smaller than the neutron separation energy for light-mass nuclei near the β-stability line. The Coulomb barrier for proton emission from the light-mass nucleus is even smaller than the difference between the proton and neutron separation energies in these nuclei. Thus proton evaporation is more favorable than neutron evaporation in the light targets (Na, S and Ca). On the other hand, in heavier nuclei, like Sr, proton emission is strongly suppressed due to the large Coulomb barrier, resulting in dominance of neutron evaporation. It should be noted that a simple direct knock-out process would give almost the same chance for proton or neutron removal, producing residual nuclei with nearly the same T_z as that of target nuclei.

A comparison of relative yields of mirror nuclei one mass number less than the $T_z = 0$ target (S and Ca) is interesting. Available data on the yield ratios for different projectiles with different energies are listed in Table 7. The ratios are larger than unity, reflecting the discussion above. We note that the ratio seems to increase as either the projectile energy decreases or its mass increases. Grover and Coretto[26)] discussed proton induced reactions in terms of a clean knock-out (CKO) process and an inelastic scattering followed by evaporation (ISE) process. The former predicts smaller values for the ratios than the latter. The ratios in Table 7 seem to be indicating that the ISE process becomes more dominant than the CKO at lower energy or with heavier-mass projectile. Recent theoretical calculations gave good agreement for the 400 MeV/N ^{12}C on the Ca target but not for the 250 MeV/N ^{12}C bombardment[24)].

4.4 Comparison with relativistic pion and proton induced reactions

It is of interest to compare especially our data on ^{40}Ca with those of other groups using different projectiles. In Fig. 9, cross sections for the N = Z even-even products (the so-called alpha-particle nuclei) are compared. These products give the most prominent gamma rays of the in-beam gamma spectra. There is a very interesting qualitative trend as one goes from light to heavy projectiles. The 220-MeV π^- projectile produces a straight exponential fall-off of cross section with decreasing mass of products. The protons, both at 210 MeV and at 600 MeV, produce a short plateau, with the yields of ^{32}S and ^{28}Si nearly equal, but otherwise an exponential decrease in yield with slope like that for pions. Our α data at 400 MeV/N show a broader plateau with masses 32, 28, and 24 nearly equal. Our carbon data show the flat plateau still broader with the ^{20}Ne yield rising to 70% that of ^{24}Mg. It should be noted that for all these experiments ^{36}Ar and ^{32}S points are subject to some ambiguity in that there are unresolved or partially resolved gamma transitions of ^{33}S and ^{30}Si, respectively. From gamma feeding considerations and theoretical calculations we expect that the ^{33}S contribution to the ^{36}Ar point is small, but the ^{30}Si correction to ^{32}S may be of the order of 40%. Thus, the plateau may have a reverse slope, with the ^{32}S yield less than ^{28}Si yield, for all but the π^- data.

It is beyond the scope of this experimental paper to discuss in detail the reasons for plateau formation with heavier projectiles. There is a substantial literature on cascade-evaporation calculations for protons on nuclei. We may, on quite general grounds, expect that in going from light to heavier projectiles

an increasing number of nucleons are knocked-out in the fast cascade (or "abrasion" step in Swiatecki's nomenclature). Thus, the pion yields represent mainly statistical nucleon and alpha evaporation from intermediate excited nuclei of ^{40}Ca or its near neighbors. The monotonic fall-off of yields reflects this feature. For our carbon data at the other extreme there must be a greater range of intermediate excited products of the fast initial collision process at various impact parameters. Thus, plateau formation in product yields results. It is not fruitful to carry the qualitative arguments much farther. In Ref. 24 complicated firestreak-model computer calculations of yields from ^{12}C on ^{40}Ca at 250 MeV/N and 400 MeV/N are presented. The theory does not give as flat a plateau region as the data, so the understanding of these peripheral reaction results is only partial.

4.5 Momentum transfer

From the Doppler broadening of a γ-ray observed at 90° to the beam, we can estimate the tranverse momentum transferred to the target fragment. We observed small (or no) broadening of the γ-lines in the spectra at 90°. Analysis of the 1.67 MeV $2^+ \rightarrow 0^+$ transition in ^{20}Ne from the Na target gave a mean transferred momentum of the order of 250 MeV/c at both 90° and 141° to the beam direction, and the Doppler shift is small. These results are consistent with the observations of projectile fragments$^{1)}$ and indicate the total linear momentum transferred to be of the order of the Fermi momentum. From this linear momentum transfer magnitude we expect a transferred angular momentum of $\Delta L \approx \Delta p \cdot r \approx 5h$.

The hope of inferring much about the average spins of the products was not realizable in the quantitative way that isomeric ratios have been used at lower bombarding energies. In only very few nuclei was more than one gamma ray observable, and that one is usually from first excited state to ground. The failure to observe 4 → 2 gamma rays in even-even products would seem to signify a rather small average spin of the products after nucleon evaporation but before the gamma cascade. We did not observe the $4^- \rightarrow 3^-$ transition in ^{38}Ar with the Ca target which the recent study[25)] of 90 MeV α bombardment on the Ca target has shown as a strong γ-ray in ^{38}Ar.

For ^{38}K formed from calcium we can essentially extract an isomeric ratio. The off-beam radioactivity measurements of Table 5 give the ^{38}K ground state yields (spin and parity 3^+), while in Table 4 the gamma ray gives directly the yield to the 0.45 MeV 1^+ state. These ratios $\sigma_{3^+}/\sigma_{1^+}$ are 2.2 for both alpha and carbon beams at 400 MeV/N. The spins are not sufficiently different to allow firm conclusions about average spins of ^{38}K formed.

For ^{37}Ar from Ca we observed in Table 5 a population ratio $\sigma_{7/2^-}/\sigma_{1/2^+}$ of 3.6 and 2.8 for alphas and carbons, respectively. As with ^{38}K, there is some favoring of the higher spin state, but not much.

4.6 Summary

i) Discrete nuclear gamma rays following relativistic heavy ion projectiles are reported here for the first time. They arise selectively from the peripheral reaction process, where the momentum and energy transferred to the residual target fragments are small.

ii) Doppler effects on the discrete gamma lines are small. The ratios of the cross-sections for producing the same target fragments by the ^{12}C and α induced reactions are around 1.2. These observations indicate the peripheral nature of the reaction. They are consistent with those observed in the projectile fragments in peripheral collisions[2)].

iii) Asymmetry of the proton and neutron removal processes and the large yield of the inelastic gamma rays show important roles of the evaporation process after the fast abrasion and target excitation processes.

iv) These reaction mechanisms with high energy (relativistic) projectiles are analogous to those with medium energy projectiles, where there is a pre-equilibrium de-excitation process followed by evaporation at the equilibrium stage[12)].

v) The cross-sections for target fragments fall off as exp $(-Q_{min}/\underline{a})$, where Q_{min} is the minimum Q value for the fragment formation. The quantity $\underline{a}$ gets larger in going from 250 MeV/N to 400 MeV/N. More nucleons (clusters) are removed in the heavy-ion induced reactions than in the proton- and pion-induced reactions. These features differ from those found in the projectile fragments[2)]. We do not attach any fundamental significance to the Q_{min} correlation and refrain from using the term "temperature" with $\underline{a}$. A correlation with mass number of product is about as good.

We are much indebted to the following people: the BEVALAC staff and operators for excellent support of experiments, Dr. J. Carroll and others of the UCLA group for their help in beam focussing and other details of operation in our shared cave at the BEVALAC, Dr. C. Wiegand and Dr. B. Berman for loan of the valuable targets, and Professor D. Shirley for making freely available the Ge(Li) and NaI(Tl) detectors used.

We are grateful to Dr. B. Harvey, Professor M. Sakai and Professor K. Sugimoto for their continuous interest and encouragement. One of us (H.E.) would like to thank the Department of Chemistry, University of California for support as a visiting professor in the fall quarter of 1975.

Appendix

Contribution from secondary particles

We used rather thick targets of 1 to 3 g/cm^2 to get a good signal-to-background ratio. For such thick targets we cannot ignore the contribution by secondary particles produced in the targets. If we had used thinner targets with more intense beam, background by the beam halo and neutrons would have become intolerable.

To study the contribution of secondary particles, we used sodium targets with thicknesses of 0.8 and 3.2 g/cm^2 and sulfur targets of 1.3 and 2.7 g/cm^2 for carbon projectiles of 400 MeV/N. Most of the secondary contribution comes from protons and neutrons because the production cross sections for these particles are much larger than for other particles[27). Since the γ-rays observed are mostly due to multi-nucleon removal reactions, contributions come mainly from high energy particles (>40 MeV) except for the inelastic scattering and few-nucleon (<2) removal reactions. Thus, the ranges of the particles which are responsible for the contribution are larger than the target thicknesses. Therefore the measured cross section σ_m can be expressed by $\sigma_m = \sigma_o(1 + bt)$, where σ_o is the net cross section, b(cm^2/g) is the contribution of secondary particles, and t is the target thickness (g/cm^2). The production cross sections for protons and neutrons increase as the mass number of the target nucleus increases, while the number of atoms per unit area for a given thickness (g/cm^2) is proportional to the inverse of the target mass number. Therefore, the value b only weakly depends on the target mass number. The γ-ray intensity ratios for various transitions with the targets of different thickness are given in Tables A1 and A2. Here the yield ratios are almost constant for all transitions for the Na and S targets, respectively, except for the 440 keV transitions in ^{23}Na produced by the inelastic scattering of the target nucleus. Since the obtained b values were almost the same for the Na and S targets, we took b = 0.08 ± 0.06 cm^2/g by averaging both results for the Na and S targets. We excluded the 440-keV inelastic γ-ray of ^{23}Na in determining the b value because the energy of the first excited state is so small (440 keV) that a tremendous number of low energy secondary neutrons contributes to this γ-ray. We used b = 0.3 ± 0.25 cm^2/g for the 440 keV transition from the Na target.

The projectile mass dependence of the proton yield has been measured for ^{20}Ne(400 MeV/N) and (400 MeV/N) by Gosset et al.27). For energetic protons (E_p > 60 MeV) the proton yield ratio between the ^{20}Ne and α projectiles is about 5, equal to the mass ratio of projectiles. Therefore we used the smaller value of 1/3 of the carbon value.

Since the b value does not depend much on the target mass, as was mentioned before, we used the same value for the Ca target. The estimated corrections to cross sections were 0.06±0.05, 0.09±.07, and 0.19±.15 for the ^{12}C(400 MeV/N) bombardment and were 0.02±.02, 0.03±.02, and 0.07±.05 for the (400 MeV/N) bombardment on the Na, S, and Ca targets, respectively.

For the inelastic γ-ray in the Na target, the corrections were 0.19 ± .17 and 0.07 ± .06 for the ^{12}C and α projectiles, respectively. We got a 22% correction for the Sr target assuming the same b value as the one obtained for the light mass targets.

Reference

1) D. E. Greiner, P. J. Lindstron, H. H. Heckman, Bruce Cork, and F. S. Bieser, Phys. Rev. Lett. 35 (1975) 152.

2) P. J. Lindstrom, D. E. Greiner, H. H. Heckman, Bruce Cork, and F. S. Bieser, Lawrence Berkeley Laboratory Report No. LBL-3650 (1975).

3) W. R. Frazer, L. Ingber, C. H. Mehta, C. H. Poon, D. Silverman, K. Stowe, P. D. Ting, and H. J. Yesian, Rev. Mod. Phys. 44 (1972) 284.

4) M. Buenerd, C. K. Gelbke, B. G. Harvey, D. L. Hendrie, J. Mahoney, A. Menchaca-Rocha, C. Olmer, and D. K. Scott, Phys. Rev. Lett. 37 (1976) 1191.

5) H. Feshbach and K. Huang, Phys. Lett. 47B (1973) 300.

6) S. Barshay, C. B. Dover, and J. P. Vary, Phys. Lett. 51B (1974) 5.

7) A. S. Goldhaber, Phys. Lett. 53B (1974) 306.

8) V. K. Lukyanov and A. I. Titov, Phys. Lett. 57B (1975) 10; V. K. Lukyanov, Y. A. Panebratsev, and A. I. Titov, Dubna Report No. E2-9089.

9) J. Hufner, K. Schafer, and B Schurmann, Phys. Rev. C 12 (1975) 1888; A. Abul-Magd, J. Hufner, and B. Schurmann, Phys. Lett. 60B (1976) 327; A. Abul-Magd and J. Hufner, Z. Physik A 277 (1976) 379.

10) G. D. Westfall, P. J. Lindstrom, D. E. Greiner, H. J. Crawford, Lance W. Wilson, and H. H. Heckman, Bull. Am. Phys. Soc. 23 (1978) 27.

11) W. Loveland, R. J. Otto, D. J. Morrissey, and G. T. Seaborg, Phys. Rev. Lett. 39 (1977) 320.

12) H. Ejiri, Y. Nagai, H. Sakai, T. Itahashi, T. Shibata, M. Hoshi, S. Nakayama, T. Kishimoto, and K. Maeda, Proc. Int. Conf. Nuclear Structure, Tokyo, 1977, J. Phys. Soc. Japan (to be published).

13) V. G. Lind, H. S. Plendl, H. O. Funsten, W. J. Kossler, B. J. Lieb, W. F. Lankford, and A. J. Buffa, Phys. Rev. Lett. 32 (1974) 479.

14) D. Ashery, M. Zaider, Y. Shamai, S. Cochavi, M. A. Moinester, A. Yavin, and J. Alster, Phys. Rev. Lett. 32 (1974) 943.

15) H. E. Jackson, D. G. Kovar, L. Meyer-Schützmeister, R. E. Segel, J. P. Schiffer, S. Vigdor, T. P. Wangler, R. L. Burman, D. M. Drake, P. A. M. Gram, R. P. Redwine, V. G. Lind, E. N. Hatch, O. H. Otteson, R. E. McAdmans, B. C. Cook, and R. B. Clark, Phys. Rev. Lett. 35 (1975) 641.

16) C. C. Chang, N. S. Wall, and Z. Fraenkel, Phys. Rev. Lett. 33 (1974) 1493.

17) O. Artun, Y. Cassagnou, R. Legrain, N. Lisbona, L. Roussel, J. I. Alard, A. Baldit, J. P. Costilhes, J. Fargeix, G. Roche, and J. C. Tamain, Phys. Rev. Lett. 35 (1975) 773.

18) R. E. Segel, L. R. Greenwood, P. Debevec, H. E. Jackson, D. G. Kovar, L. Meyer-Shutzmeister, J. E. Monahan, F. J. D. Serduke, T. P. Wangler, W. M. Wharton, and B. Zeidman, Phys. Rev. C 13 (1976) 1566.

19) M. Sadler, J. Jastrzebski, A. Nadasen, and P. P. Singh, L. L. Rutledge, Jr., T. Chen, and R. E. Segel, Phys. Rev. Lett. 38 (1977) 950.

20) J. B. Cumming, Ann. Rev. Nucl. Sci. 13 (1963) 260.

21) A. R. Smith and R. H. Thomas, Lawrence Berkeley Report LBL-3861 (1975).

22) R. Anholt, J. Ioannou-Yannou, H. Bowman, E. Rauscher, S. Nagamiya, J. O. Rasmussen, T. Shibata, and H. Ejiri, Phys. Lett. 59 A (1977) 429.

23) P. M. Endt and C. Van der Leun, Nucl. Phys. A214 (1973) 1.

24) J. O. Rasmussen, R. Donangelo, and L. F. Oliveira, Proc. Symp. on Macroscopic Features of Heavy Ion Collisions and Pre-equilibrium Process, Hakone (1977) 440.

25) T. Shibata et al. private communication (1977).

26) J. R. Grover and A. A. Carretto, Jr., Ann. Rev. Nucl. Sci. 14 (1964) 51.

27) J. Gosset, H. H. Gutbrod, W. G. Meyer, A. M. Poskanzer, A. Sandoval, R. Stock, and G. D. Westfall, Phys. Rev. C 16 (1977) 629.

Figure captions

Fig. 1. Schematic drawing of experimental set-up.

Fig. 2. Time structure of Bevatron beam and gate positions for prompt-, delayed, and off-beam spectra.

Fig. 3. Gamma-ray spectrum following the ^{23}Na(^{12}C,X)Y reaction at $E_{^{12}C}$ = 4.8 GeV. The γ-rays denoted by letters a through f are as follows: a 511 keV, b 596 keV ^{74}Ge(n,n'γ), c 690 keV ^{72}Ge(n,n'γ), d 835 keV ^{54}Mn, e 846 keV ^{27}Al, f 1137 keV and 1332 keV ^{60}Co.

Fig. 4. Gamma-ray spectrum following the ^{nat}S(^{12}C,X)Y reaction at $E_{^{12}C}$ = 4.8 GeV. (See the figure caption in Fig. 3 for the γ-rays denoted by a to f.)

Fig. 5. Gamma-ray spectrum following the ^{nat}Ca(α,X)Y reaction at E_α = 1.6 GeV(See the figure caption in Fig. 3 for the γ-rays denoted by a to f.)

Fig. 6. The relative yield for the $2^+ \rightarrow 0^+$ transition in doubly even nuclei produced by the ^{12}C bombardment at 250 MeV/N.

Fig. 7. The absolute cross sections for the $2^+ \rightarrow 0^+$ transitions in doubly even nuclei produced by the ^{12}C bombardment at 400 MeV/N.

Fig. 8. The cross section ratios between ^{12}C and α bombardments at 400 MeV/N. Dashed lines are 1.25, 1.22, and 1.21, respectively, for the Na, S, and Ca targets obtained by the expresssion $\sigma \propto A_P^{1/3} + A_T^{1/3} - 1.6$.

Fig. 9. Comparison with pion and proton data for α-particle nuclei. Closed triangles: 220 MeV π^-(ref. 15). Open

circles: 4.8 GeV ^{12}C (present work). Open squares: 1.6 GeV α (present work). Closed squares: 600 MeV protons (ref. 17).

TABLE 1

Summary of Experimental Conditions for the Three Major Runs

	Run 1	Run 2	Run 3
Beam	12.6 GeV ^{12}C 3.0 GeV ^{12}C	3.0 GeV ^{12}C	4.8 GeV ^{12}C 1.6 GeV
Target	Sr 3.5 g/cm^2 CF_2, 2.6 g/cm^2 ^{207}Pb 3.7 g/cm^2	Na 3.1 g/cm^2 S 2.7 g/cm^2 Ca 2.9 g/cm^2	Na 0.8, 3.1 g/cm^2 S 1.3, 2.7 g/cm^2 Ca 2.9 g/cm^2
Ge(Li) Detector (angle)	3mmPlanar(90°) 25ccCoaxial(90°) 30ccCoaxial(128°)	25ccCoaxial(90°) 30ccCoaxial(141°)	25ccCoaxial(90°) 30ccCoaxial(141°)
Data taking	4k PHA 8k PHA	4k PHA 8k PHA	PDP 11/10 6 x 2k
Beam Extraction	With r.f.	Without r.f.	With r.f.
Spectrum	In-beam Delayed	In-beam Delayed	In-beam Delayed Offbeam

TABLE 2

Relative γ-ray Intensities from Sr Target

Product	E_γ(keV)	Transition	I_γ a)	I_γ a)
			$E_{^{12}C}$=3.0GeV	$E_{^{12}C}$=12.6GeV
^{88}Sr	1836	$2^+ \rightarrow 0^+$	100 ± 27 b)	100 ± 36
	898	$3^- \rightarrow 2^+$	65 ± 18	33 ± 21
^{86}Sr	1076	$2^+ \rightarrow 0^+$	49 ± 12	55 ± 23
	1153	$4^+ \rightarrow 2^+$	38 ± 19	64 ± 24
^{84}Sr	793	$2^+ \rightarrow 0^+$	35 ± 14	< 27
^{82}Kr	776	$2^+ \rightarrow 0^+$	27 ± 14	

a) The intensities are values for the natural Sr target.

b) The absolute cross section for the 1836 keV is 78 ± 34mb.

TABLE 3 Gamma-ray yields from the sodium Target

Product	E_γ(keV)	Transition	σ_α(mb) E_α = 1.6 GeV	σ_C(mb) $E_{^{12}C}$ = 4.8 GeV	σ_C(arbitrary) $E_{^{12}C}$ = 3.0 GeV
^{23}Na	440	$5/2^+ \rightarrow 3/2^+$	18.9 ± 3.3	23.7 ± 5.4	79 ± 27
^{22}Na	583	$1^+ \rightarrow 3^+$	14.7 ± 2.5	19.6 ± 4.0	76 ± 10
	891	$4^+ \rightarrow 3^+$	4.3 ± 1.1	3.5 ± 1.6	
^{22}Ne	1275	$2^+ \rightarrow 0^+$	23.8 ± 4.3	29.1 ± 6.2	110 ± 23
^{21}Ne	351	$5/2^+ \rightarrow 3/2^+$	22.6 ± 3.6	24.7 ± 4.1	100 ± 11
^{20}Ne	1634	$2^+ \rightarrow 0^+$	19.2 ± 3.6	20.0 ± 4.1	100 ± 24
^{19}Ne	238	$5/2^+ \rightarrow 1/2^+$	1.3 ± 0.5	1.8 ± 1.3	
^{18}F	937	$3^+ \rightarrow 1^+$	4.4 ± 1.2	8.9 ± 2.9	
^{18}O	1983	$2^+ \rightarrow 0^+$	7.2 ± 2.1	4.9 ± 2.1	

TABLE 4 Gamma-ray yields from the sulfur target

Product	E_γ(keV)	Transition	σ_α(mb)	σ_c(mb)	σ_c(arbitrary)	σ_p(arbitrary)[a)]
			E_α=1.6GeV	$E_{^{12}C}$=4.8GeV	$E_{^{12}C}$=3.0GeV	E_p=218MeV
$^{32}S+^{30}Si$	2230	$2^+ \rightarrow 0^+$	56.6 ± 8.8	70.4 ± 12.7	100 ± 5	18.9
^{31}S	1249	$3/2^+ \rightarrow 1/2^+$	8.5 ± 1.6	10.3 ± 2.5	10.0 ± 2.1	14.3
^{31}P	1266	$3/2^+ \rightarrow 1/2^+$	21.0 ± 3.2	23.0 ± 4.6	51.6 ± 3.2	23
^{30}P	709	$1^+ \rightarrow 1^+$	5.8 ± 1.1	10.3 ± 3.6	8.0 ± 1.6	5.3
^{29}Si	2028	$5/2^+ \rightarrow 1/2^+$	15.2 ± 3.0	15.2 ± 3.5	17.1 ± 2.0	
^{28}Si	1779	$2^+ \rightarrow 0^+$	28.7 ± 4.6	38.5 ± 7.6	48.4 ± 4.6	19.7
^{26}Al	417	$3^+ \rightarrow 5^+$	8.6 ± 1.2	9.7 ± 2.1	7.0 ± 1.5	2.9
^{26}Mg	1809	$2^+ \rightarrow 0^+$	9.5 ± 1.5	14.0 ± 3.2	19.5 ± 2.8	
^{25}Al	452	$1/2^+ \rightarrow 5/2^+$	2.4 ± 0.5	3.4 ± 1.2		
^{24}Mg	1369	$2^+ \rightarrow 0^+$	16.6 ± 2.6	22.4 ± 4.0	24.0 ± 2.6	
^{24}Na	472	$1^+ \rightarrow 4^+$	5.8 ± 1.2	10.3 ± 2.4		9
^{23}Na	440	$5/2^+ \rightarrow 3/2^+$	14.0 ± 2.1	15.9 ± 3.0	13.6 ± 1.8	
^{22}Na	583	$1^+ \rightarrow 3^+$	9.1 ± 2.6	8.2 ± 2.5	14.2 ± 4.0	
^{22}Ne	1275	$2^+ \rightarrow 0^+$	13.1 ± 2.0	17.0 ± 3.9	15.2 ± 5.5	

continued

TABLE 4 (continued)

^{21}Ne	351	$5/2^+ \rightarrow 3/2^+$	10.8±1.5	12.9±2.3	7.3±1.3
^{20}Ne	1634	$2^+ \rightarrow 0^+$	8.1±1.5	13.5±3.2	10.7±2.7

a) ref. 17

TABLE 5 Gamma-ray yields from the calcium target

Product	E_γ(keV)	Transition	σ_α(mb)	σ_c(mb)	σ_c(arbitrary)	σ_p(mb)$^{a)}$
			E_α=1.6GeV	$E_{^{12}C}$=4.8GeV	$E_{^{12}C}$=3.0GeV	E_p=210M
^{40}Ca	3737	$3^- \to 0^+$	7.2±2.4	14.4±4.4	25.6±10.3	13.4
^{39}Ca	2796	$7/2^- \to 3/2^+$	6.2±1.8	5.7±2.7	< 7	8.5
^{39}K	2814	$7/2^- \to 3/2^+$	6.5±1.8	10.8±3.3	38.8±12.5	9.7
^{38}K	328	$1^+ \to 0^+$	9.0±1.5	11.1±2.7	17.3± 7.1	8.3
^{38}Ar	2168	$2^+ \to 0^+$	9.1±2.4	15.2±4.2	85.2±18.7	10.9
^{37}Ar	1611	$7/2^- \to 3/2^+$	16.1±2.9	16.9±5.9	66.2±10.3	13.6
	1410	$1/2^+ \to 3/2^+$	4.5±1.3	6.1±2.2		
^{36}Ar+^{33}S	1970	$2^+ \to 0^+$	28.6±4.6	38.6±8.6	100 ± 17	28.4
^{36}Ar+^{38}Ca	2208	$3^- \to 2^+$	19.9±4.7	24.3±6.2	78.3±14.9	
^{36}Cl	789	$3^+ \to 2^+$	11.6±2.0	14.6±2.8	10.9± 5.4	
^{35}Cl	1763	$5/2^+ \to 1/2^+$	9.1±2.1	8.1±2.5	10.2± 7.3	
^{35}S	1570	$1/2^+ \to 3/2^+$	2.8±1.4	5.1±2.2		
^{34}S	2127	$2^+ \to 0^+$	9.4±4.3	13.2±6.3	44.9±16.9	
^{32}S+^{30}Si	2230	$2^+ \to 0^+$	16.4±3.3	23.5±6.3	100 ± 21(^{32}S)	16.6
^{32}Si	1941	$2^+ \to 0^+$	9.5±2.8	7.7±2.5		
^{31}S	1249	$3/2^+ \to 1/2^+$			14.3± 5.4	
^{31}P	1266	$3/2^+ \to 1/2^+$	13.2±2.3	15.1±4.0	76.5± 8.9	
^{30}P	709	$1^+ \to 1^+$	3.5±1.0	4.4±1.5	9.5± 4.8	
^{30}Si	2235	$2^+ \to 0^+$			32.8±13.3	
^{29}Si	2028	$5/2^+ \to 1/2^+$	7.3±3.5	6.4±2.9	17.7± 9.7	
^{28}Si	1779	$2^+ \to 0^+$	17.3±3.3	22.0±5.6	53.4±11.1	16.7
^{26}Al	417	$3^+ \to 5^+$	4.4±1.3	7.4±2.0	5.2± 4.6	
^{26}Mg	1809	$2^+ \to 0^+$	11.6±2.8	16.5±4.7	17.0± 6.7	
^{24}Mg	1369	$2^+ \to 0^+$	14.9±2.8	20.5±6.5	57.2± 7.9	
^{24}Na	472	$1^+ \to 4^+$	5.1±1.2	7.1±2.9		
^{23}Na	440	$5/2^+ \to 3/2^+$	9.9±1.9	11.9±3.3	34.5± 7.1	
^{22}Na	583	$1^+ \to 3^+$	5.7±1.8	5.4±2.5	19.1± 6.0	
^{22}Ne	1275	$2^+ \to 0^+$	6.5±2.3	7.6±2.9		
^{21}Ne	351	$5/2^+ \to 3/2^+$	7.9±1.4	12.7±3.0	8.4± 6.0	
^{20}Ne	1634	$2^+ \to 0^+$	5.4±1.6	14.0±4.2	21.7± 8.4	

a) ref. 17

TABLE 6

Cross Sections for Radioactivities Produced by α(400 MeV/N) and ^{12}C(400 MeV/N) Bombardment

Product	Target	Eγ(keV)	σ_{α}(mb)	$\sigma_{^{12}C}$(mb)
^{20}F	Na	1634	11.9 ± 2.6	16.1 ± 3.0
^{28}Al	S	1779	12.0 ± 2.4	15.1 ± 3.4
^{38}K	Ca	2167	20.1 ± 3.6	24.9 ± 4.6
^{34m}Cl	Ca	2127	11.7 ± 2.7	13.3 ± 4.2
^{28}Al	Ca	1779	10.5 ± 2.5	11.4 ± 2.4

TABLE 7: Yield Ratios for Single-Proton to Single-Neutron Removal Processes.

	p 210 MeV a)	α 400 MeV	^{12}C 400 Mev	^{12}C 250 MeV
<u>Ca Target</u>				
$Y(^{39}K)/Y(^{39}Ca)$	1.1	1.1 ± 0.5	1.9 ± 1.1	>5.15
<u>S Target</u>				
$Y(^{31}P)/Y(^{31}S)$	1.6	2.5 ± 0.6	2.2 ± 0.7	5.2 ± 1.1

a) From reference 17.

TABLE A1. Cross section ratios for the Na targets with 3.1 g/cm^2 and 0.8 g/cm^2 bombarded by ^{12}C(400 MeV/N).

Product	E_γ (keV)	$\sigma_m(3.1\ g/cm^2)/\sigma_m(0.8\ G/cm^2)$
^{23}Na	440	1.54 ± 0.31
^{22}Na	583	1.23 ± 0.30
^{22}Ne	1275	1.15 ± 0.31
^{21}Ne	351	1.14 ± 0.23
^{20}Ne	1634	1.22 ± 0.34

TABLE A2. Cross section ratios for the S target with 2.7 g/cm^2 and 1.3 g/cm^2 bombarded by ^{12}C(400 MeV/N).

Product	E_γ (keV)	$\sigma_m(2.7\ g/cm^2)/\sigma_m(1.7\ g/cm^2)$
^{32}S	2230	1.14 ± 0.26
^{31}S	1249	1.27 ± 0.39
^{31}P	1266	1.31 ± 0.33
^{29}Si	2028	1.24 ± 0.47
^{28}Si	1779	1.14 ± 0.28
^{26}Al	417	0.99 ± 0.28
^{26}Mg	1809	1.05 ± 0.32
^{24}Mg	1369	1.10 ± 0.26
^{23}Na	440	0.99 ± 0.24
^{21}Ne	351	1.00 ± 0.24

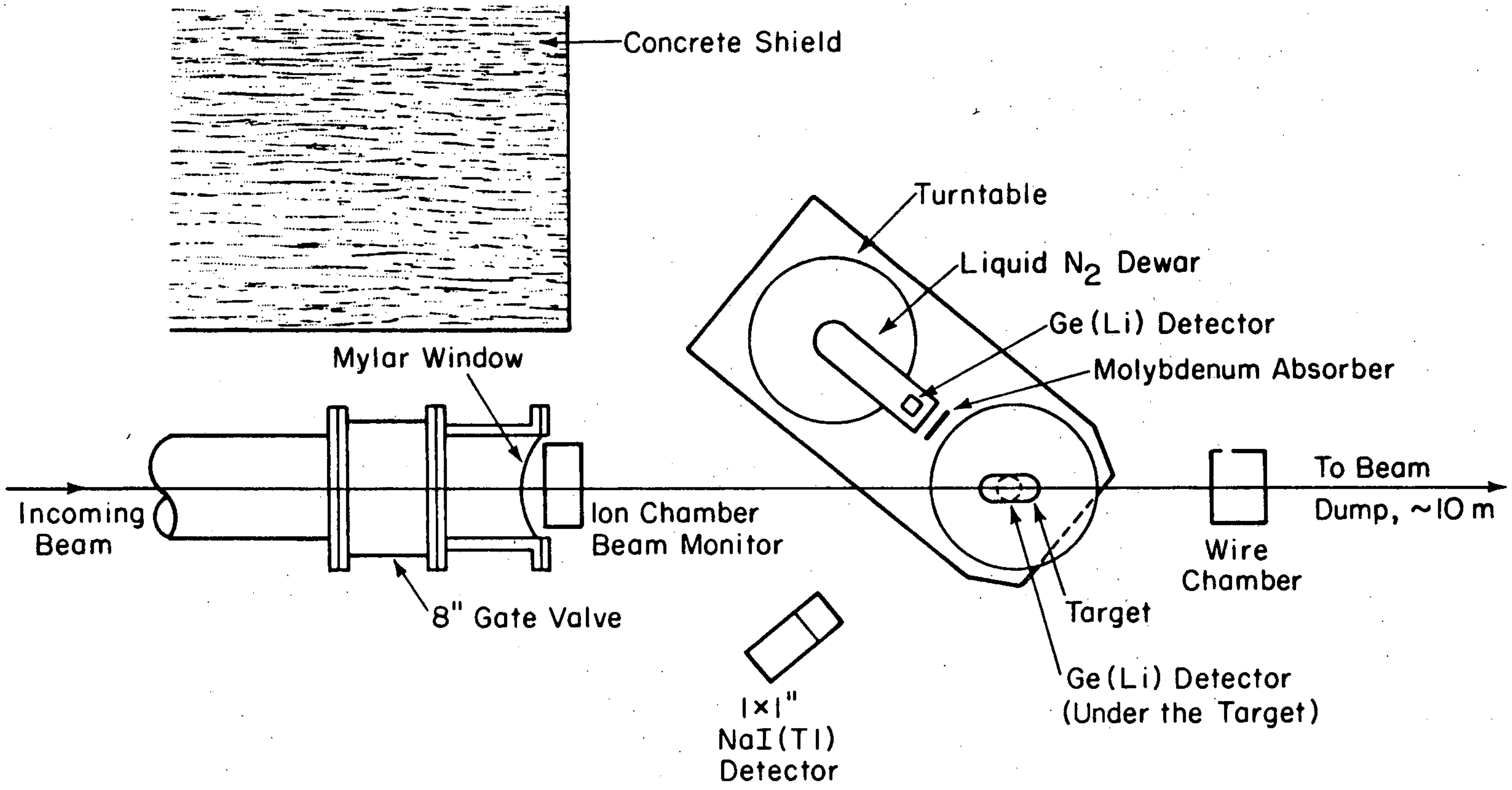

XBL 776-8896

Fig. 1

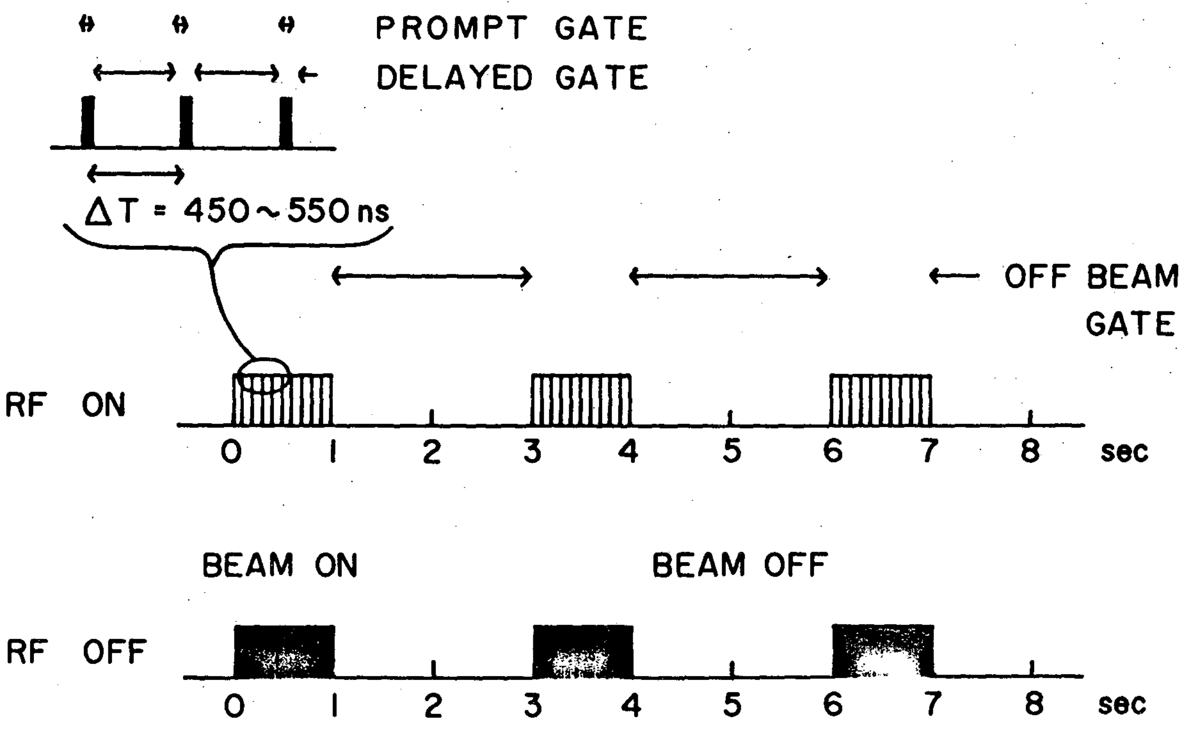

XBL 781-6893

Fig. 2

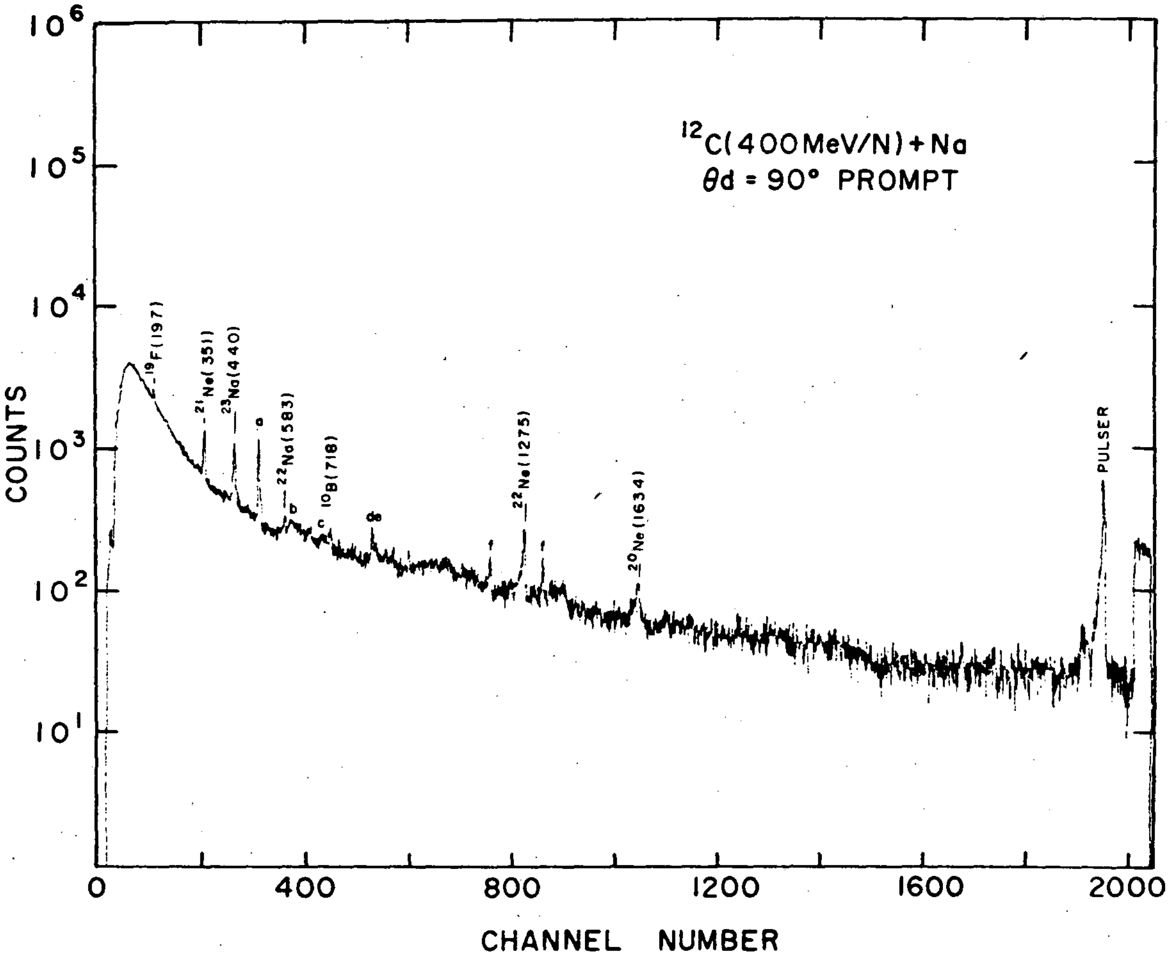

XBL 781-7039

Fig. 3

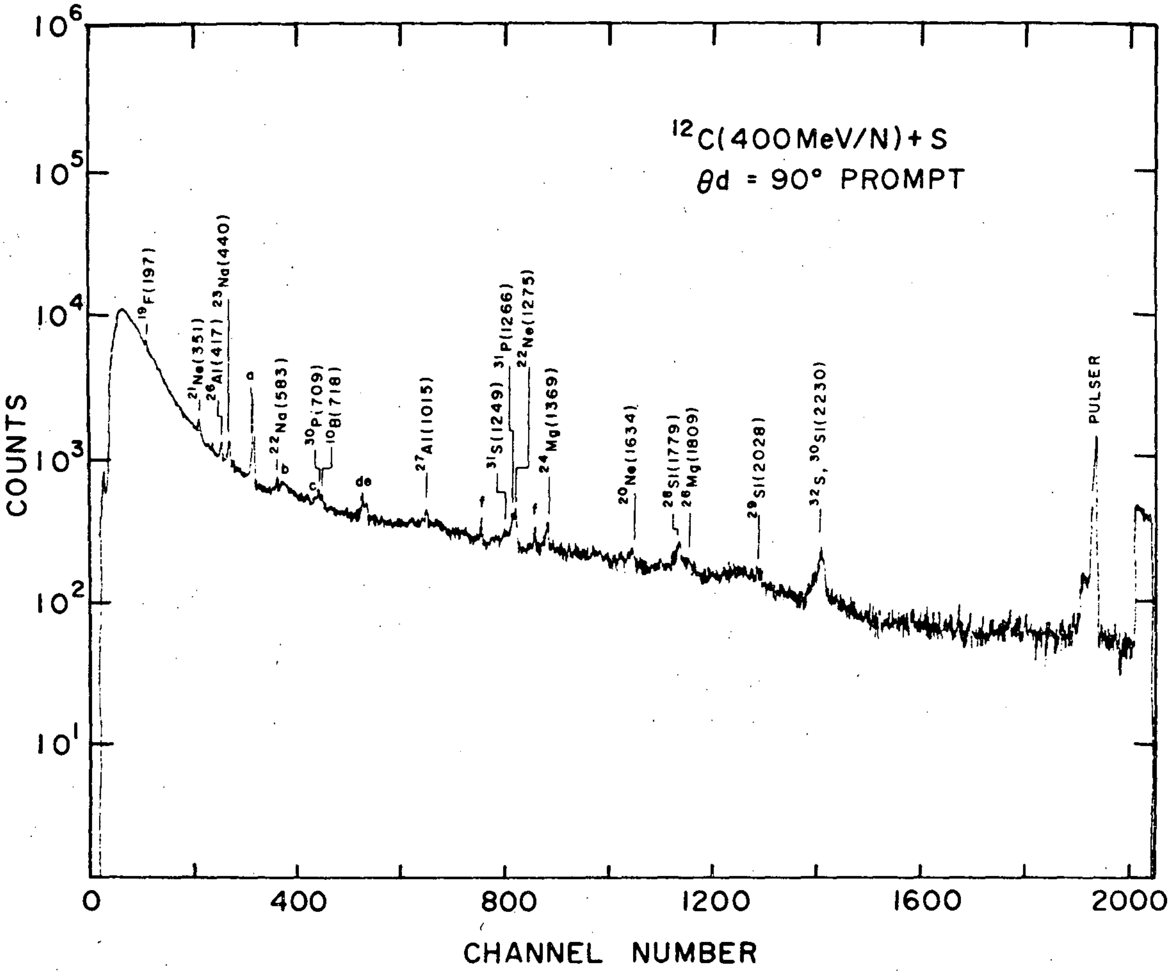

XBL 781-7038

Fig. 4

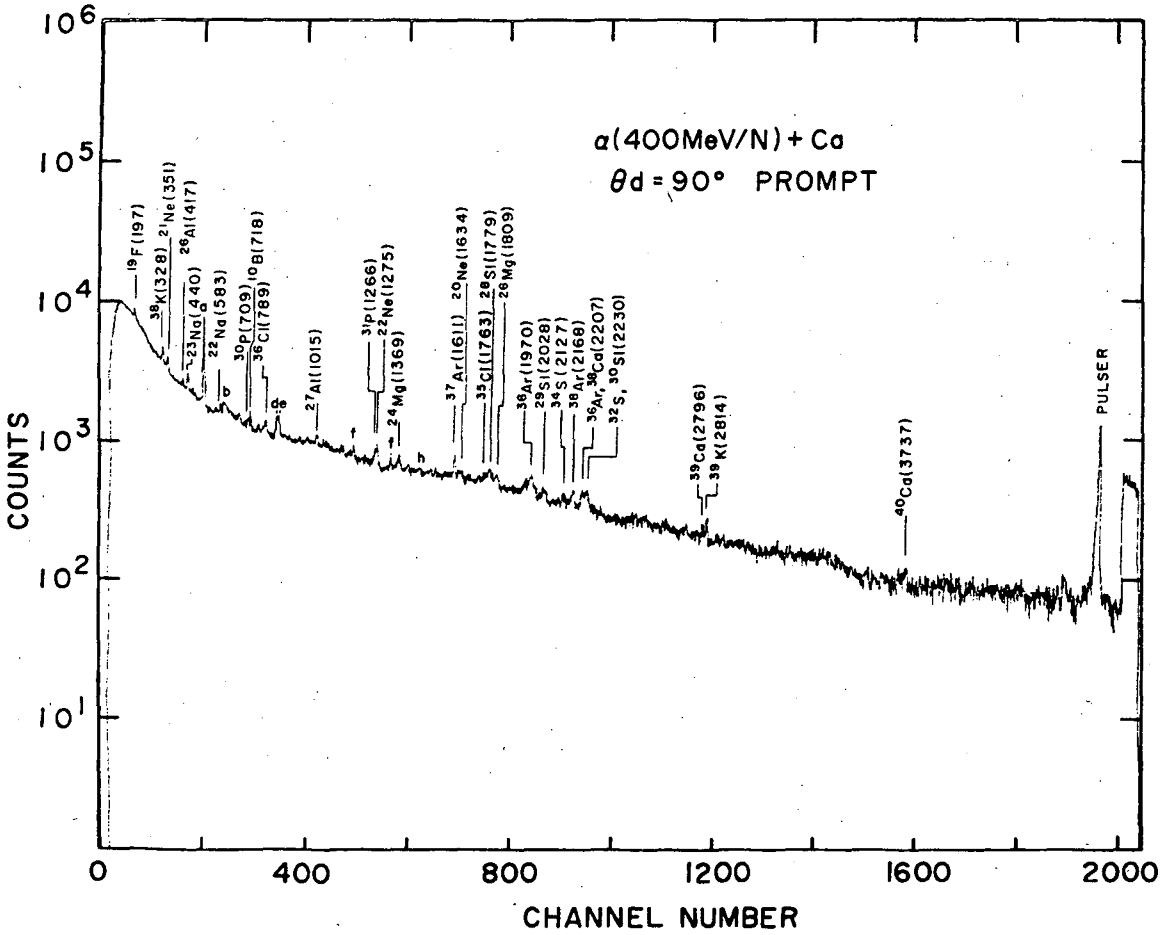

XBL 777-9606

Fig. 5

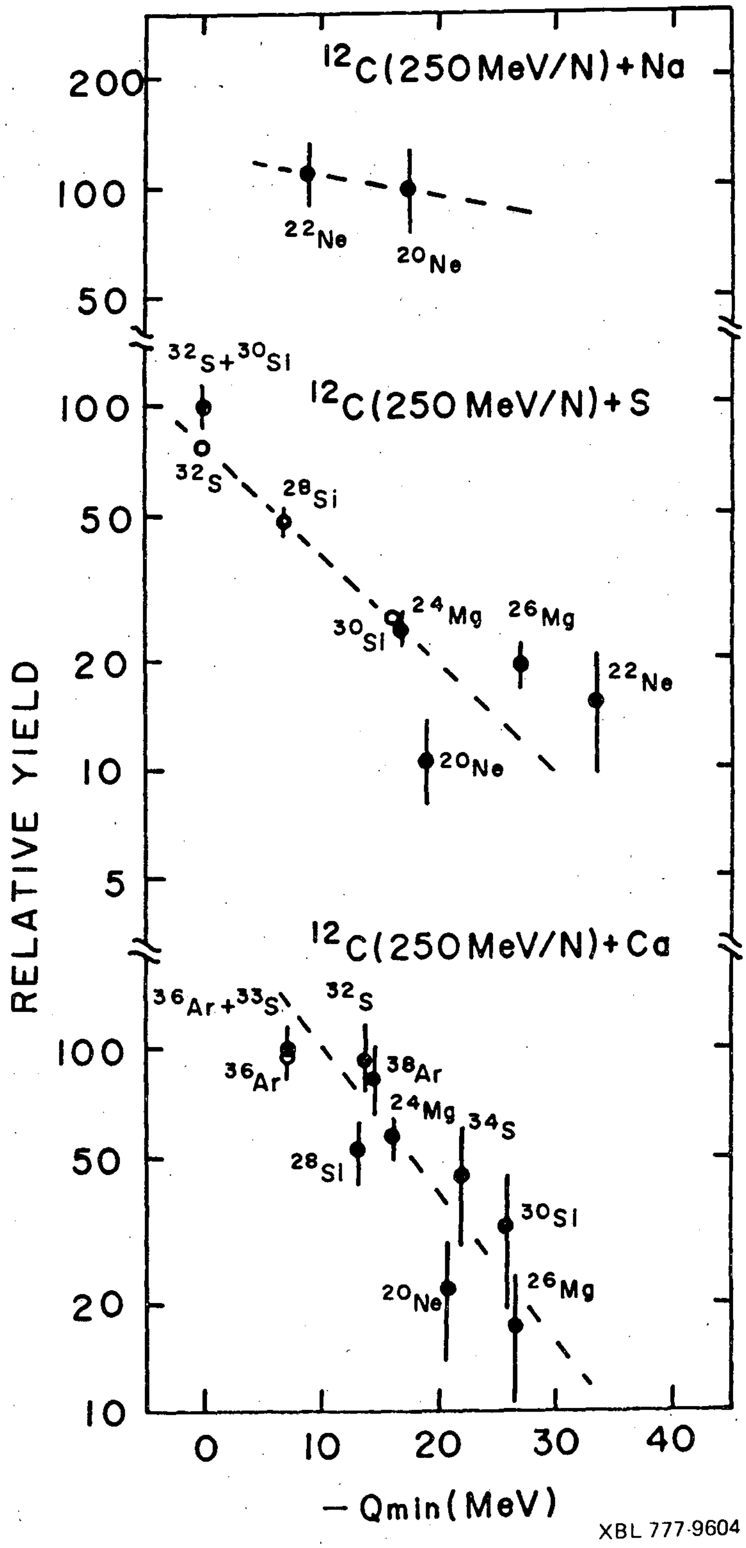

^{12}C(250MeV/N)+Na
^{22}Ne
^{20}Ne
^{12}C(250 MeV/N)+S
^{32}S+^{30}Si
^{32}S
^{28}Si
^{24}Mg
^{30}Si
^{26}Mg
^{22}Ne
^{20}Ne
^{12}C(250MeV/N)+Ca
^{36}Ar+^{33}S
^{36}Ar
^{32}S
^{38}Ar
^{24}Mg
^{34}S
^{28}Si
^{30}Si
^{20}Ne
^{26}Mg
RELATIVE YIELD
200
100
50
100
50
20
10
5
100
50
20
10
0
10
20
30
40
− Qmin(MeV)
XBL 777-9604

Fig. 6

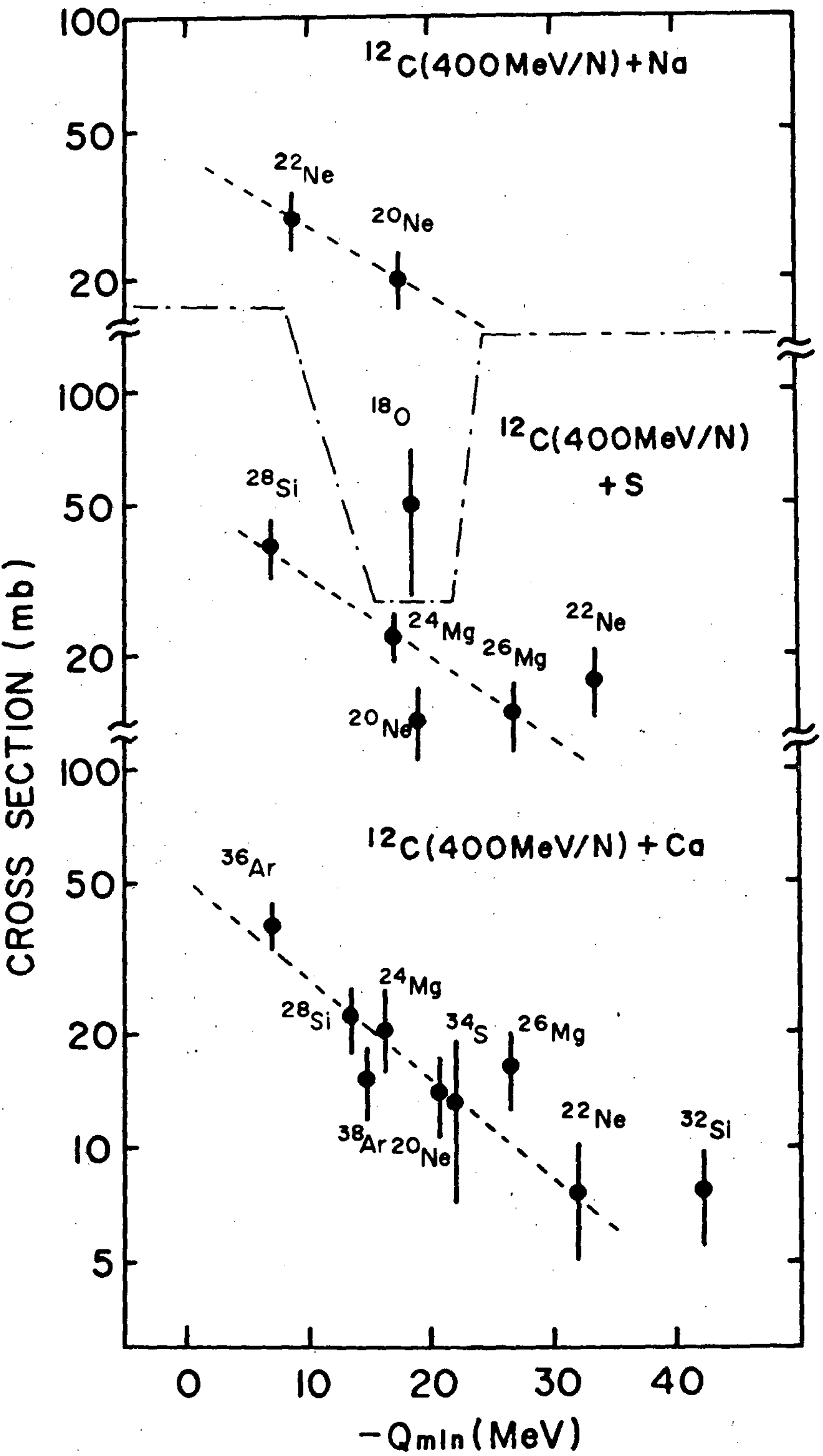

XBL 7711-10663

Fig. 7

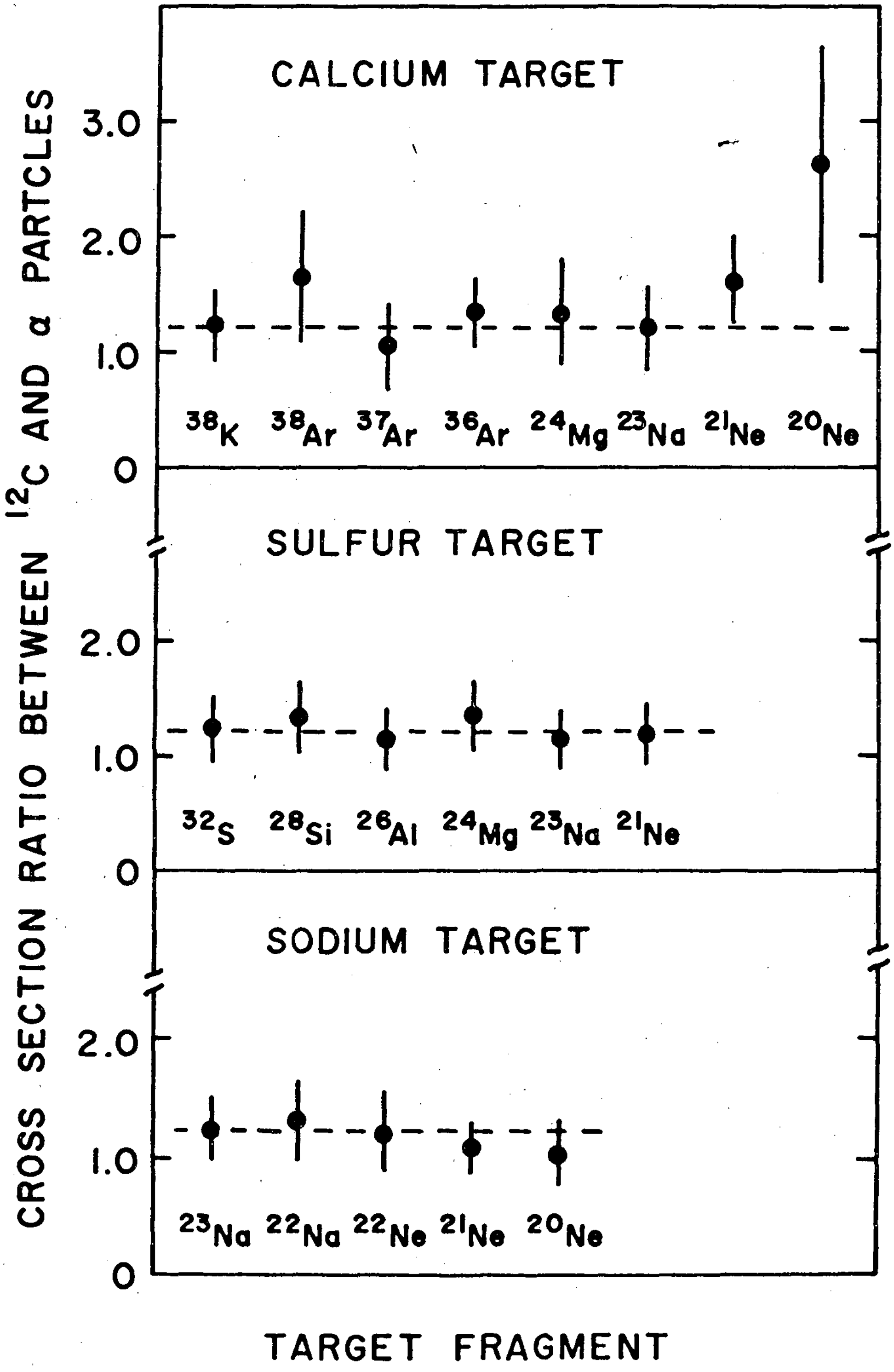

XBL 7711-10662

Fig. 8

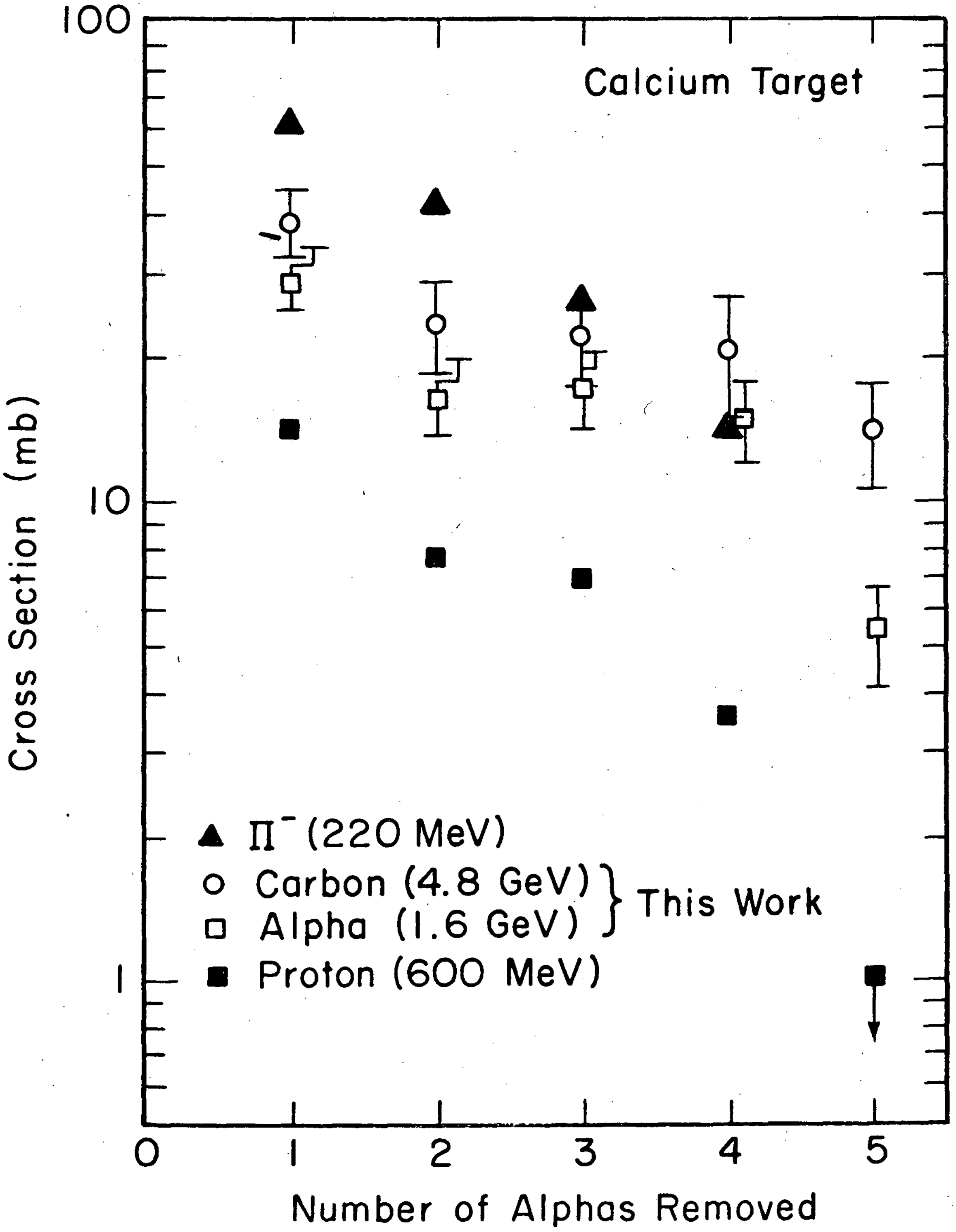

XBL 776-8895

Fig. 9

TECHNICAL INFORMATION DEPARTMENT
LAWRENCE BERKELEY LABORATORY
UNIVERSITY OF CALIFORNIA
BERKELEY, CALIFORNIA 94720